Rolling Ribbons

P. S. Raux,[1] P. M. Reis,[1] J. W. M. Bush,[1] and C. Clanet[2]
[1]Department of Mathematics, Massachusetts Institute of Technology, Cambridge, Massachusetts 02139, USA
[2]LadHyX, École Polytechnique, 91128 Palaiseau, France
(Received 23 March 2010; published 23 July 2010)

We present the results of a combined experimental and theoretical investigation of rolling elastic ribbons. Particular attention is given to characterizing the steady shapes that arise in static and dynamic rolling configurations. In both cases, above a critical value of the forcing (either gravitational or centrifugal), the ribbon assumes a two-lobed, peanut shape similar to that assumed by rolling droplets. Our theoretical model allows us to rationalize the observed shapes through consideration of the ribbon's bending and stretching in response to the applied forcing.

DOI: 10.1103/PhysRevLett.105.044301 PACS numbers: 46.70.De, 46.25.−y, 46.35.+z

Galileo's study of rigid spheres rolling down an inclined ramp [1] is often considered as the starting point of modern physics, since it involves both theory and experiment [2,3]. The influence of ramp flexibility on the dynamics was recently considered by Aristoff *et al.* [4]. We here consider another variant of Galileo's problem in which the ramp is rigid but the rolling body, an elastic cylindrical shell, is deformable. As will be shown, this dynamical elastic problem presents some common features with the rolling of a liquid drop on a hydrophobic surface [5–7] or a lubricated ramp [8]. We first present our experimental observations and then develop a supporting theoretical model.

The ribbons are cast out of three different types of vinylpolysiloxane that produce three elastic polymers with Young's moduli $E = 0.26$ MPa, 0.56 MPa and 1.2 MPa, and respective densities $\rho = 1050$ kg/m^3, 1100 kg/m^3, and 1200 kg/m^3. The associated Poisson ratio is measured to be $\nu = 0.5$. The geometrical characteristics of the ribbons are radius $R_0 = (23.2 \pm .4)$ mm, length $L_0 = 2\pi R_0$, thickness $(0.8 < h_0 < 3.25)$ mm, width $(18 < w_0 < 28)$ mm, cross sectional area $S_0 = h_0 w_0$ and momentum of inertia $I_0 = \frac{1}{12} w_0 h_0^3$ [Fig. 1(f)]. With this system, it is possible to vary the bending stiffness EI_0 by a factor 400 (from 2×10^{-7} N $\cdot$ m^2 to 8×10^{-5} N $\cdot$ m^2) by adjusting the ribbon thickness h_0. Since the rolling ribbon stretches at high speeds, the stretched properties are denoted by R, L, h, w, S and I, respectively.

To examine the rolling states, the ribbon is placed on the inner surface of a hollow, rotating stainless steel drum of radius $R_{\text{drum}} = 150$ mm, this drum being a practical alternative to Galileo's ramp. Because of frictional forces between the polymer and stainless steel, there is no slippage between the drum and the ribbon, which is thus driven at a constant speed U prescribed by the drum. Typical steady, rolling shapes are presented in Figs. 1(a)–1(d). As the drum speed increases, the ribbon assumes progressively more distorted equilibrium shapes up to a critical speed at which periodic waves appear on its surface [Fig. 1(e)]. The critical "touchdown" speed is reached when the upper and the lower ribbon surfaces come into contact. Since these surfaces move in opposite directions, their contact generally leads to complex time-dependent motions, for example, waves propagating in the opposite direction of rotation, ribbon bouncing, or even the sticking of the ribbon to the wall. Figure 1(g) presents the evolution of the observed ribbon shapes with increasing speed (blue denotes the static case, dark red the critical touchdown speed). Our goal now is to understand physically and describe theoretically the evolution of the shape with the rotation speed.

Even in the absence of rotation, the ribbons may deform in response to gravity [Fig. 1(a)]. To quantify this static deformation with a single quantity, we introduce the aspect

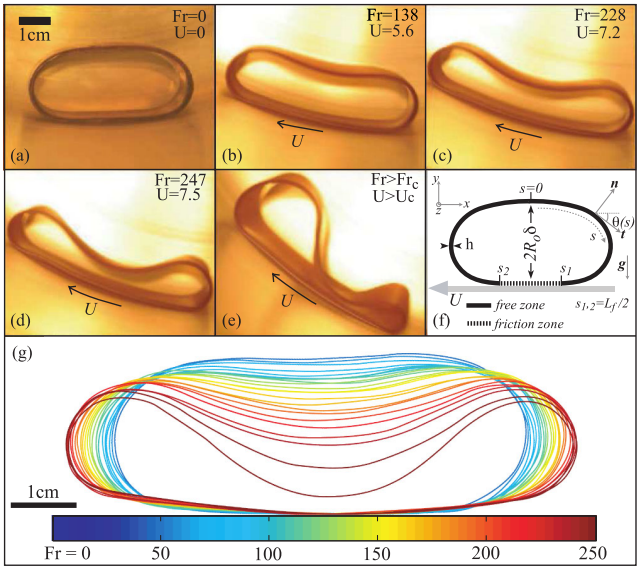

FIG. 1 (color online). A ribbon rolling at different speeds [or Froude number $\text{Fr} = U^2/(gR_0)$]: (a) Fr = 0, (b) Fr = 143, (c) Fr = 236 (d) Fr = 259, (e) An unsteady shape observed above the critical touchdown speed. (f) A schematic of the ribbon. (g) Experimentally observed dependence of ribbon shape on Froude number. Ribbon properties: $E = 0.26$ MPa, $\rho = 1050$ kg/m^3, $h = 1.6$ mm, $w = 27$ mm.

ratio $\delta = \frac{H}{2R_0}$ where H is the height at the middle of the ribbon [Fig. 1(f)]. Note that $\delta = 1$ when the ribbon is undeformed, and $\delta = \frac{h}{R_0}$ at touchdown. The balance between gravitational energy $\rho S_0 R_0^2 g$ and bending energy EI_0/R_0 indicates a characteristic length scale $L_g = (EI_0/\rho g S_0)^{1/3}$ beyond which one expects substantial deformation. Small values of L_g/R_0 will be associated with large ribbon deformations, large values with a circular shape. In Fig. 2, we present the evolution of the aspect ratio δ with $\Gamma_g = (L_g/R_0)^3$. In the range $\Gamma_g > 4$, the circular shape is only weakly affected by gravity while strong deformations are observed for $\Gamma_g \leq 1$. Touchdown is achieved at $\Gamma_g^\star = 0.19$. The observed dependence of static ribbon shape on Γ_g is rationalized in our subsequent theoretical developments.

We observe that, as the speed increases, the rolling ribbon develops a two-lobed shape. A similar behavior has been reported for rotating liquid drops [7,9]. As the drop rotation speed increases, its shape evolves through a series of axisymmetric forms, from a sphere to an oblate ellipsoid to a torus. However, above a critical speed, the axisymmetric equilibrium shape is no longer adopted [10,11], and the drop assumes a two-lobed, peanut shape. The critical rotation speed Ω_L above which a drop of radius R_L loses its axisymmetry is found to scale as $\sqrt{\gamma_L/\rho_L R_L^3}$, where γ_L and ρ_L are the surface tension and density, respectively. This scaling emerges from balancing the destabilizing rotational energy $\rho_L R_L^5 \Omega_L^2$ with the stabilizing surface energy $\gamma_L R_L^2$. Drawing an analogy between the liquid drop and our elastic ribbon suggests that the latter will lose its axisymmetric form when its rotational energy $\rho S_0 R_0^3 \Omega_c^2$ greatly exceeds its elastic energy EI_0/R_0. Thus, even in the absence of the flattening influence of gravity, one anticipates deformed ribbons for velocities larger than $\sqrt{E/\rho}h_0/R_0$. For the ribbon presented in Fig. 1, this critical velocity is of the order of 1 m/s, which is substantially less than that observed experimentally ($U_c \approx 7.5$ m/s). This discrepancy has motivated the more precise analysis detailed below.

Guided by the scaling analysis, we characterize the ribbon deformation in terms of the parameter $\Gamma_i = Eh^2/\rho R_0^2 U^2$ to study the ribbon deformation. We note that stretching is important in our experiments; thus, we define Γ_i in terms of h instead of h_0. The observed variation of δ with Γ_i is reported in Fig. 3. In the zero velocity limit ($\Gamma_i \to \infty$), the aspect ratio tends towards the static value imposed by Γ_g. Since the results presented in Fig. 3 correspond to four different ribbons with four different values of Γ_g, we observe four different asymptotic values. We observe in Fig. 3 that the aspect ratio differs substantially from its static limit only for $\Gamma_i \leq 1$. In the large velocity limit ($\Gamma_i \to 0$), the deformation increases ($\delta \to 0$) up until touchdown at $\Gamma_i^\star$, the value of which depends on Γ_g. Typically, $\Gamma_i^\star \approx 0.02$. One way to show that $\Gamma_i^\star$ indeed depends on Γ_g is to consider the limit of a ribbon for which $\Gamma_g = \Gamma_g^\star$. In this limit, touchdown is achieved without any rotation, that is for $U = 0$ or $\Gamma_i^\star = \infty$. Apart from this

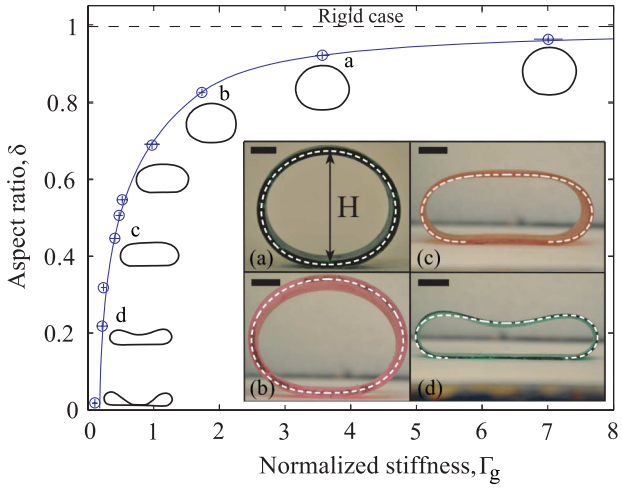

FIG. 2 (color online). Aspect ratio of static ribbons, $\delta = \frac{H}{2R_0}$, as a function of their normalized stiffness $\Gamma_g = \frac{EI_0}{\rho g S_0 R_0^3}$. The line is deduced by integrating Eq. (7) with Fr = 0. For the letters on the curve, we present in the inset the corresponding picture. The theoretical shape obtained through numerical integration of Eq. (7) is superposed as a thin white dashed line. Scale bars, 10 mm.

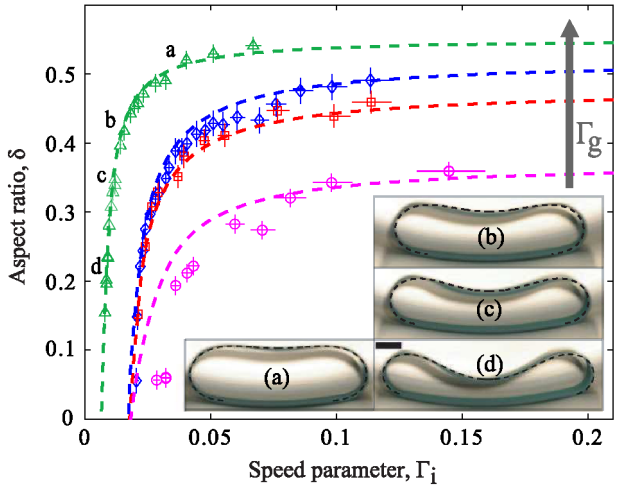

FIG. 3 (color online). Aspect ratio, $\delta = \frac{H}{2R_0}$, of different rolling ribbons as a function of the speed parameter $\Gamma_i = \frac{Eh^2}{\rho R_0^2 U^2}$. Curves correspond to those predicted by Eq. (7). Circles, squares, diamonds, and triangles correspond to four different ribbons; specifically, $\Gamma_g = 0.278$, 0.372, 0.429, 0.488. $E = 0.26$ MPa for the first three ribbons and $E = 0.56$ MPa for the last. Inset: Shape comparison for a single ribbon ($R_0 = 22.8$ mm, $\Gamma_g = 0.488$, $E = 0.56$ MPa) at different rotation speeds: (a) $Cy = 0.09$, (b) $Cy = 0.16$, (c) $Cy = 0.20$, (d) $Cy = 0.25$, where $Cy = \rho U^2/E$. Dashed curves are computed by integration of Eq. (7). Scale bar: 10 mm.

dependence of the critical velocity on the initial gravitational deformation of the ribbon, we observe that, qualitatively, the shape transition prompted by centripetal forces is similar to that caused by gravity and presented in Fig. 2. We proceed with a quantitative study, by developing a theoretical model that predicts the steady shapes of both static and rolling ribbons.

A schematic diagram of the ribbon system is presented in Fig. 1(f). The ribbon shape is described in terms of the arc length s along its center line. Let $\underline{n}$ be the outward pointing unit vector normal to the ribbon, θ the angle between the local tangent vector $\underline{t}$ and the horizontal unit vector $\underline{e}_x$. Considering the ribbon as a slender elastic structure, the local force and torque balances can be expressed as [12]:

$$\underline{F}' = -\underline{K}, \tag{1}$$

and

$$EI\theta'' = \underline{F} \times \underline{n}, \tag{2}$$

where $\underline{F}$ represents the internal forces and $\underline{K}ds$ the external ones. Primes denote derivatives with respect to s. To integrate this system, we divide the ribbon into two zones where the external constraints $\underline{K}$ are different: a contact zone and a free zone. In the free zone ($-L_f/2 < s < L_f/2$, where L_f is the free length), there is no friction, but gravitational and centripetal forces act. In the contact zone ($|s| > L_f/2$), friction pins the ribbon to the drum. Consequently, the ribbon has a small but finite curvature prescribed by that of the drum: its center line is in translation at a constant speed $U(\frac{R}{R+\frac{h}{2}})$.

In the free zone, the external force acting on an infinitesimal element of ribbon has both gravitational and centripetal contributions:

$$\underline{K} = \rho S\underline{g} + \rho SU^2\theta'\underline{n}. \tag{3}$$

In order to determine boundary conditions for the vertical and horizontal components of the internal force, F^y and F^x respectively, we assume that the shape is symmetric with respect to the vertical midplane, an assumption consistent with experimental observations prior to touchdown of the ribbon. It is thus sufficient to consider one half of the ribbon. The symmetry also sets the boundary conditions at the top of the ribbon where the shape must be perpendicular to the axis of symmetry ($\theta|_{s=0} = 0$) and where there is no variation of curvature ($\theta''|_{s=0} = F^y|_{s=0} = 0$). We also assume continuity with the contact zone, which is insured by applying additional boundary conditions: a flat contact zone for the static case ($\theta|_{s=L_f/2} = \pi$ and $\theta'|_{s=L_f/2} = 0$) and a small curvature corresponding to that of the drum for the dynamic case ($\theta|_{s=L_f/2} = \pi - \arcsin(\frac{x|_{s=L_f/2}}{R_{\text{drum}}})$ and $\theta'|_{s=L_f/2} = \frac{1}{R_{\text{drum}}}$). The internal force can be found by integrating (1) using (3),

$$\underline{F}(s) = \begin{pmatrix} F^x \\ F^y \end{pmatrix} = \begin{pmatrix} F^x|_{s=0} + \rho SU^2[\cos\theta|_s - 1] \\ -\rho gSs - \rho SU^2 \sin\theta|_s \end{pmatrix}. \tag{4}$$

Since the tension in the ribbon is equal to the tangential component of the internal force, we have $\underline{F} \times \underline{t} = ES\frac{(ds-ds_0)}{ds_0}$ where $ds - ds_0$ is the extension of the ribbon. Integrating this equation and combining it with (4) yields the increase of the ribbon's free length:

$$L_f - L_{f_0} = C_y \int \left[1 + \left(\frac{\Phi}{\text{Fr}} - 1\right)\cos\theta + \frac{\bar{s}}{\text{Fr}}\sin\theta\right] ds_0. \tag{5}$$

Here, $\bar{s} = \frac{s}{R_0}$ denotes the nondimensional curvilinear coordinate, and L_{f_0} the free length at rest. The Cauchy number $C_y = \frac{\rho U^2}{E}$ indicates the relative magnitude of inertial and stretching forces while the Froude number $\text{Fr} = \frac{U^2}{gR_0}$ expresses that of inertia and gravity. Finally, $\Phi = \frac{F^x|_{s=0}}{\rho gSR_0}$ is the ratio between the tension at rest and gravity. This tension depends on the natural curvature of the ribbon. Since our ribbons are molded, their natural curvature is close to $1/R_0$ and the tension is close to zero in the absence of gravity. In our numerical integration, we take this information into account by choosing the smallest possible value of Φ.

Since θ varies from 0 to 2π along the free length, the cosine and sine terms in (5) are much smaller than the constant after integration; thus, the stretching is uniform to leading order. In the contact zone, where there is no sliding, we extend the assumption of uniform stretching over the whole ribbon, so the total extended length L is given by

$$L = (1 + C_y)L_0. \tag{6}$$

The variation of thickness due to transverse stretching is deduced from the Poisson ratio, $\nu = 0.5$: since our polymer conserves volume, the ribbon thickness, $h = h_0(1 - \nu C_y)$, necessarily decreases with increasing speed. In order to determine the shape of the free length, we substitute (4) into (2), which after nondimensionalization yields

$$(1 - \nu C_y)^2\Gamma_g\theta'' = (\text{Fr} - \Phi)\sin\theta - \bar{s}\cos\theta \tag{7}$$

where $\Gamma_g = \frac{EI_0}{\rho gS_0R_0^3}$ again prescribes the relative magnitudes of bending and gravity.

We use a combined fourth and fifth order explicit Runge-Kutta method to integrate (7) numerically between $s = 0$ and the first value of s that satisfies the condition $s + x|_s = L/2$ where L is the stretched length given by (6). We use a shooting method, and close the system by adjusting the values of Φ and $\theta'|_{s=0}$ to match the slope $\theta|_{s=L_f/2}$ and curvature $\theta'|_{s=L_f/2}$ of the substrate at the edge of the contact zone. We thus obtain the ribbon shape, $\theta(s)$, by integrating (7) with no fitting parameter.

We first compare our model and experiments in the static (Fr = 0) case. In Fig. 2, we present the shapes calculated

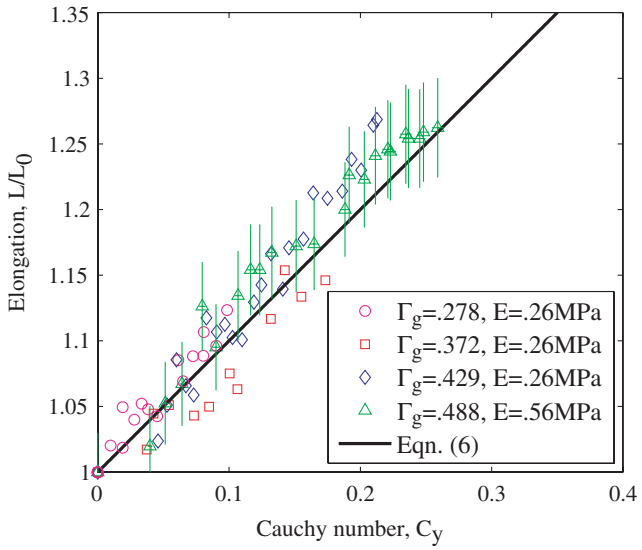

FIG. 4 (color online). Ribbon elongation as a function of the Cauchy number $C_y = \frac{\rho U^2}{E}$. The black line is the dependence predicted by Eq. (6). Different symbols correspond to different values of normalized stiffness Γ_g. Characteristic error bars are shown for only one set of experiments.

from (7) and see good agreement between theory and experiment for the four different ribbons considered. We proceed by verifying our assumption of constant stretching along the rolling ribbon. In Fig. 4, we present the dependence of length extension, $\frac{L}{L_0}$, on the Cauchy number for four different ribbons. Despite the uncertainty in ribbon length introduced by the image analysis, a linear fit of the experimental results gives a slope close to that predicted by (6) within a 6% margin of error. The observed stretching is thus consistent with our hypothesis of uniform extension.

For rolling ribbons, the curves in Fig. 3 represent the prediction obtained by integrating (7) for the values of Γ_g corresponding to the observed deformation at rest, that is, the asymptotic value of δ at large Γ_i. The discrepancies observed near the critical touchdown speed are likely due to the climbing of the ribbon along the inner wall of the rotating cylinder, and the resulting fore-aft asymmetry of the ribbon. In the dynamic case, we also compare observed and predicted ribbon shapes, as presented in the inset of Fig. 3 for four different values of C_y on the same ribbon, which necessarily has a single Γ_g value. As in the static case, the agreement between observed and predicted shapes is satisfactory.

We have considered the rolling of elastic ribbons and shown that their shape results from a delicate coupling between rolling, bending, and stretching. While we have noted that the rolling ribbon has several features common with rolling droplets [6–8], a similar family of shapes has also been reported for tumbling blood cells [13], a tube collapsing under uniform pressure [14], and carbon nanotubes deformed by van der Waals forces [15,16]. The rationale for similar shape progressions emerging in these disparate physical systems has yet to be carefully considered, but should be informed by our study.

[1] G. Galilei, *Dialogues Concerning Two New Sciences* (Dover Publications Inc., New York, NY., 1954).
[2] H. F. Cohen, *The Scientific Revolution: A Historiographical Inquiry* (The University of Chicago Press, Chicago, USA, 1994).
[3] S. Drake, N. M. Swerdlow, and T. H. Levere, *Essays On Galileo And The History And Philosophy Of Science* (University of Toronto Press, Toronto, Canada, 1999).
[4] J. M. Aristoff, C. Clanet, and J. W. M. Bush, Proc. R. Soc. A **465**, 2293 (2009).
[5] L. Mahadevan and Y. Pomeau, Phys. Fluids **11**, 2449 (1999).
[6] P. Aussillous and D. Quéré, Nature (London) **411**, 924 (2001).
[7] P. Aussillous and D. Quéré, J. Fluid Mech. **512**, 133 (2004).
[8] S. R. Hodges, O. E. Jensen, and J. M. Rallison, J. Fluid Mech. **512**, 95 (2004).
[9] L. Elkins, P. Ausillous, J. Bico, D. Quere, and J. W. M. Bush, Meteorit. Planet. Sci. **38**, 1331 (2003).
[10] R. A. Brown and L. E. Scriven, Proc. R. Soc. A **371**, 331 (1980).
[11] Lord Rayleigh, Philos. Mag. **28**, 161 (1914).
[12] L. D. Landau and E. M. Lifshitz, *Theory Of Elasticity*, Course of Theoretical Physics, Vol. 7 (Pergamon Press, Oxford, 1986).
[13] J. M. Skotheim and T. W. Secomb, Phys. Rev. Lett. **98**, 078301 (2007).
[14] J. E. Flaherty, J. B. Keller, and S. I. Rubinow, SIAM J. Appl. Math. **23**, 446 (1972).
[15] T. Hertel, R. E. Walkup, and P. Avouris, Phys. Rev. B **58**, 13 870 (1998).
[16] A. Pantano, D. M. Parks, and M. C. Boyce, J. Mech. Phys. Solids **52**, 789 (2004).